THE JOURNAL OF PHYSICAL CHEMISTRY A
A JOURNAL OF THE AMERICAN CHEMICAL SOCIETY

pubs.acs.org/JPCA

Article

Formation of a Resonance-Stabilized Radical Intermediate by Hydroxyl Radical Addition to Cyclopentadiene

Kacee L. Caster, James Lee, Zachery Donnellan, Talitha M. Selby, David L. Osborn, and Fabien Goulay*

Cite This: *J. Phys. Chem. A* 2022, 126, 9031−9041

Read Online

ACCESS | Metrics & More | Article Recommendations | Supporting Information

ABSTRACT: The reaction of the OH radical with cyclopentadiene (C_5H_6) was investigated at room temperature using multiplexed photoionization mass spectrometry. OH radicals in their ground electronic state were generated in the gas phase by 248 nm photolysis of H_2O_2 or 351 nm photolysis of HONO. Analysis of photoion spectra and temporal profiles reveal that at room temperature and over the 4−8 Torr pressure range, the resonance-stabilized 5-hydroxycyclopent-2-en-1-yl (C_5H_6OH) is the main observed reaction product. Abstraction products (C_5H_5) were not detected. The C_5H_6OH potential energy surface calculated at the CCSD(T)/cc-pVTZ//M06-2X/6-311++G** level of theory suggests that the resonance-stabilized radical product is formed through barrierless addition of the OH radical onto cyclopentadiene's π system to form a van der Waals complex. This weakly bound adduct isomerizes through a submerged energy barrier to the resonance-stabilized addition adduct. Master Equation calculations, including two OH-addition entrance pathways, predict that 5-hydroxycyclopent-2-en-1-yl remains the sole addition product up to 500 K. The detection of an OH-containing resonance-stabilized radical at room temperature further highlights their importance in carbon- and oxygen-rich environments such as combustion, planetary atmospheres, and the interstellar medium.

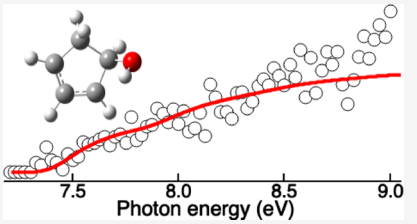

1. INTRODUCTION

Resonance-stabilized radicals (RSRs) containing a hydroxyl group have been identified as primary products during the OH radical-initiated oxidation of small unsaturated and aromatic molecules.[1−5] They are characterized by the delocalization of an unpaired electron in a molecular π-orbital. Participation of the OH group with the delocalized π electrons may further stabilize the radical. RSRs play a significant chemical role in oxygen-rich gas-phase environments (e.g., interstellar medium, planetary atmospheres, and combustion)[1,6−11] due to their resistance to oxidation by molecular oxygen. Reaction of an RSR with O_2 forms a peroxy radical at the expense of localizing the previously delocalized electron, leading to a weak C−O_2 bond. The newly formed bond in these peroxy radicals is likely to thermally dissociate at lower temperatures than peroxy radicals of non-resonance-stabilized radicals, therefore increasing the propensity of RSRs to accumulate.[12−14] In combustion, self-recombination and cross-recombination reactions of RSRs typically lead to the formation of the first aromatic ring from which molecular weight growth to polycyclic aromatic hydrocarbon formation occurs.[15−22] At low and intermediate temperatures, OH-containing radicals are likely to be formed by addition of the OH radical onto unsaturated hydrocarbons.[23−26]

The reaction mechanism for the OH radical reaction with unsaturated hydrocarbons is well established.[1,2,25,27,28] At low and intermediate temperatures, it proceeds through the barrierless formation of a van der Waals (VdW) complex between the OH radical and the molecule's π system. The OH radical can then bond to one of the double-bonded carbon atoms through an energy barrier slightly above that of the VdW complex. In the case of OH addition onto a conjugated double bond, the resulting reaction adduct may be stabilized by resonance. As conjugation length in the hydrocarbon species increases, it is more likely that OH radical addition will lead to the formation of an RSR adduct. Resonance-stabilized addition adducts have lower energy barriers for OH addition than non-resonance-stabilized adducts.[27] The adduct may then isomerize and dissociate by H-loss to form substitution products, although at sufficiently high pressures collisional quenching by the buffer gas will prevent further isomerization. At higher temperatures, the weakly bonded VdW complex rapidly dissociates back to the reactants, making OH addition a minor entrance channel, while abstraction of a H-atom to form a hydrocarbon radical (which may itself be resonance-stabilized) and a water molecule becomes the dominant channel. The absence of energy barriers for formation of the initial VdW complex leads to a negative temperature dependence at low temperatures and room temperature, whereas the abstraction process displays an Arrhenius behavior. Competition between the addition and abstraction mechanisms leads to a rate coefficient that decreases from low

Received: September 29, 2022
Revised: November 8, 2022
Published: November 23, 2022

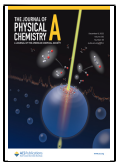

https://doi.org/10.1021/acs.jpca.2c06934
J. Phys. Chem. A 2022, 126, 9031−9041

to intermediate temperatures to a minimum value before increasing at high temperatures. The temperature corresponding to the minimum value of the rate coefficient typically ranges between 500 and 1000 K.[29,30] Stabilization of the addition adduct and formation of an OH-containing radical is therefore a likely reaction pathway in gas-phase environments such as the interstellar medium (ISM) and planetary atmospheres.

Several experimental and theoretical studies have investigated the reaction of the OH radical with conjugated hydrocarbons.[3,31−33] For OH addition onto isoprene ($H_2C{=}C(CH_3){-}HC{=}CH_2$), the resonance-stabilized OH addition adduct has been shown to play a central role in the isoprene atmospheric oxidation mechanism.[3,23,24,32] In the case of acrolein ($H_2C{=}CH{-}HC{=}O$), the simplest conjugated carbonyl-containing molecule, addition of the OH radical onto one of the carbons of the vinyl group followed by O_2 addition leads to the formation of two different peroxy radicals.[34] The location of the radical site after OH addition governs the O_2 addition mechanism and the structure of the final oxidation products. When OH adds to the terminal carbon of acrolein, the vinoxy-like radical is stabilized through resonance. Reaction of this adduct with molecular oxygen is expected to be much slower than that with the non-resonance-stabilized radical formed by OH addition to the other carbon atom of the C=C bond.[12−14] Investigating the formation of RSRs by OH reactions with conjugated molecules is therefore paramount for improving hydrocarbon oxidation chemical schemes.

Cyclopentadiene (C_5H_6, Scheme 1) is an abundant conjugated cyclic hydrocarbon which has been detected during the pyrolysis of toluene ($C_6H_5CH_3$), benzyl radical ($C_6H_5CH_2$),[35] and the jet fuel JP-10.[36] In the ISM, cyclopentadiene has recently been detected in the molecular cloud TMC-1.[37] The reaction of the CN radical with cyclopentadiene is also believed to be one of the main sources of the recently detected cyano-cyclopentadiene (C_5H_5-CN).[38,39] RSRs formed by reaction of cyclopentadiene with OH radicals in the ISM have the propensity to propagate the radical chemical scheme and accelerate molecular weight growth. The kinetics of the OH + cyclopentadiene reaction have been estimated at room temperature[40] and investigated experimentally at high temperatures.[30,41] The reaction rate coefficient ranges from 0.1 to 10×10^{-11} cm^3 s^{-1} from 300 to 1390 K with a maximum value at room temperature and a minimum value at ∼450 K. Due to the C_{2v} symmetry of cyclopentadiene, carbons 2 and 5 are equivalent, positioned α to the sp^3 hybridized carbon 1. Carbons 3 and 4 in the β position to carbon 1 are also equivalent. Overall, there are three carbon sites on cyclopentadiene for OH radical reactions to occur. Mai et al.[42] recently performed an exhaustive computational investigation of the OH + cyclopentadiene reaction. Computed branching ratios show that at room temperature, the sole reaction product is expected to be the RSR 5-hydroxycyclopent-2-en-1-yl formed by addition of the OH radical on carbon 2 (see Scheme 1) of cyclopentadiene. OH addition is the main reaction mechanism below 450 K, whereas abstraction of a hydrogen atom to form cyclopentadienyl (C_5H_5) and a water molecule dominates at higher temperatures.[41]

Scheme 1. Cyclopentadiene Carbon Labeling

Direct detection of OH addition adducts is experimentally challenging due to their reactivity and low number density. Several studies have reported the formation and detection of OH-containing radicals in complex plasma discharges[1,5] or through photolysis of a radical precursor,[32,43] but evidence of radical adduct formation by OH reactions is scarce. Loison et al.[25] reported the direct ionization of the OH-propene and OH-butene adducts (non-resonance-stabilized) using single photon ionization. At room temperature, the H-loss channel is found to be only a minor channel. The authors used 10.54 eV photons to ionize the radical adducts, and although this is considered soft ionization, most hydrocarbon radicals have adiabatic ionization energies below 9.0 eV[25,44] and start to dissociate upon ionization even at energies as low as 10.54 eV. Identifying the isomeric structures of the stabilized OH-hydrocarbon adducts therefore requires a careful analysis of the fragmentation patterns.

In the present study, tunable vacuum ultraviolet (VUV) radiation is used to ionize OH + cyclopentadiene reaction products close to their ionization threshold. Time traces of the detected masses are used to discriminate between OH + cyclopentadiene products and products from side reactions. The isomeric structures of the reaction products are determined by fitting the photoion spectra with calculated integrated Franck−Condon factors. At room temperature, it is found that the OH-containing RSR 5-hydroxycyclopent-2-en-1-yl is the sole addition product with no evidence of hydrogen abstraction pathways. Master Equation (ME) calculations are compared to the experimental data and used to predict the product branching fractions at higher temperatures. The results are also compared to recent computational results on the same system.[42]

2. EXPERIMENTAL PROCEDURE

The experiments are performed at the Advanced Light Source synchrotron at the Lawrence Berkeley National Laboratory in a low-pressure flow tube (4−8 Torr) at room temperature coupled to time-of-flight mass spectrometry. The experimental apparatus has been described in detail elsewhere[45,46] and only an abbreviated description is presented here. The cyclopentadiene reactant and OH precursor molecules (hydrogen peroxide (H_2O_2) or nitrous acid (HONO)) are injected in an excess of helium buffer gas flowing into a 62 cm slow-flow quartz reaction tube with a 1.05-cm inner diameter. Conditions in the flow tube are held at pressures between 4 and 8 Torr and at 298 K with a total gas flow rate ranging between 100 and 250 sccm. Multiple data sets using a 248 nm photolysis laser with cyclopentadiene and without OH radical precursors were collected at 373 K in a previous study.[47] Argon or krypton (for $h\nu$ < 7.9 eV) are used in a gas filter to absorb harmonics of the undulator radiation. For data recorded below 8.0 eV with argon in the gas filter, a MgF_2 window is placed in the path of the ionizing radiation to suppress harmonics of the undulator fundamental photon energy.

Gas composition and molar flow rates are regulated by mass flow controllers, whereas pressure in the flow tube is regulated by a feedback-controlled butterfly valve throttling a mechanical pump that evacuates the flow tube. A uniform concentration of OH radicals is generated down the flow tube by irradiating the gas mixture with an unfocused 248 nm (for the H_2O_2

https://doi.org/10.1021/acs.jpca.2c06934
J. Phys. Chem. A 2022, 126, 9031−9041

precursor) or 351 nm (for the HONO precursor) excimer laser at 10 Hz (for the H_2O_2 precursor) or 4 Hz (for the HONO precursor) repetition rate. The laser fluence inside the flow tube is ∼20 to 40 mJ cm^{-2}. The flow velocity is set such that the gas mixture is replenished between each laser pulse. The gas mixture is sampled about halfway down the length of the flow tube through a 650-micron diameter pinhole. The resulting molecular beam is skimmed via a 0.15 cm diameter skimmer and then ionized by tunable VUV synchrotron radiation. A 50 kHz orthogonal-acceleration time-of-flight mass spectrometer is used to monitor the resulting ions in relation to the excimer laser pulse. The resulting time-resolved mass spectra are normalized for variations in the VUV photon flux.

Hydrogen peroxide vapors are introduced into the reaction flow by passing 40% of the total helium buffer gas through a solid H_2O_2−urea complex mixed with sand and heated to 45 °C in a water bath. To avoid decomposition of H_2O_2 on metal surfaces, the gas line between the H_2O_2−urea complex reservoir and the flow tube is made of polytetrafluoroethylene and the valves are made of glass. Assuming H_2O_2 at its saturation vapor pressure,[48] the maximum possible number density of hydrogen peroxide in the reaction flow is ∼3×10^{15} molecules cm^{-3}. Using known absorption cross sections for H_2O_2 photolysis[49] and a conservative value for a H_2O_2 number density of 3×10^{14} molecules cm^{-3},[50] the OH number density is estimated to be ∼1×10^{12} molecules cm^{-3}. HONO is synthetized by flowing 20 sccm of helium gas first through a room-temperature bubbler containing a 6 M HCl solution and then through a flask containing solid $NaNO_2$. The solid sample is continuously stirred to avoid surface passivation of the sample. The pressure is maintained at ∼165 Torr in the HCl bubbler and ∼15 Torr in the $NaNO_2$ flask. The resulting gaseous mixture is directly introduced into the reaction flow tube and mixed with the reactants. HONO production is optimized by monitoring the HONO signal at m/z 47 and the NO signal at m/z 30 while adjusting the bubbler pressures. Comparison of the OH + CPD product signals between the two precursors suggests an OH number density about 10 times lower at 351 nm than at 248 nm.

Cyclopentadiene is prepared through thermal cracking of dicyclopentadiene ($C_{10}H_{12}$), and vacuum transferred into a 3.79 L stainless-steel cylinder. A detailed description of the cyclopentadiene synthesis and purification procedure has been given previously.[47] The gaseous sample at ∼90 Torr is pressurized with helium buffer gas to approximately 2000 Torr for a final mixture containing 4.0−4.5% cyclopentadiene. The resulting number density of cyclopentadiene in the reaction flow tube was approximately 5.7×10^{13} molecules cm^{-3}.

3. COMPUTATIONAL METHODS

3.1. Electronic Structure Calculations. Electronic structure calculations were performed using the Gaussian 16 (G16) suite of programs.[51] For all neutral and cationic species, a relaxed scan of the dihedral angle containing the OH group was performed at the M06-2X/6-311++G** level to determine the global minimum energy configuration.[52,53] The energy of the considered species is then calculated by reoptimizing the global minimum of each internal rotor potential at the B3LYP/CBSB7[51,54] level, and the electronic energy is calculated using the CBS-QB3 method.[55] In the case that the cation structure cannot be optimized (such as that of the 2-hydroxycyclopent-3-en-1-yl radical, INT2), the vertical ionization energy is calculated by using the neutral geometry for the cation energy calculation.

Simulated Franck−Condon factors (FCFs) were calculated at room temperature with the G16 package within the Franck−Condon approximation.[56] The calculated FCFs were convolved with a Gaussian response function (FWHM = 0.025 eV). The geometries were those optimized at the M06-2X/6-311++G** level. Because photoionization is a vertical process, in the FCF calculations, the dihedral angle of the OH internal rotor for the cation was set to that of the neutral species in the harmonic oscillator approximation. In most cases, this configuration of the cation corresponds to a local minimum on the internal rotor potential. The internal rotor potentials for the 5-hydroxycyclopent-2-en-1-yl (INT1) neutral and cationic species are displayed in Figure S1. The difference in energy between the electronic states was set to the difference in energy between the global minima of each internal rotor potential to account for any nonvertical transitions. Photoionization spectra were simulated by integrating the calculated FCF spectra. A more rigorous approach for FCF calculation has been proposed by Voronova et al.[57] and involves solving the 1D Schrodinger equation using the internal rotor potential and calculating the wavefunction overlap. Within the experimental energy resolution, the harmonic approximation used here still allows identification of the isomer products by the shape of the simulated photoion spectrum.

Stationary points on the C_5H_6 + OH potential energy surface (PES) were calculated using the G16 suite of programs. The lowest energy conformer geometries were optimized at the M06-2X/6-311++G** level using an ultrafine grid. First-order saddle points were found by scanning bond lengths or angles between intermediates. The transition-state structures were confirmed by the presence of a single imaginary frequency and by performing intrinsic reaction coordinate calculations at the same level of theory. Final single-point energy calculations were performed using the CCSD(T)/cc-pVTZ level of theory. All energies were corrected for zero-point energy from the M06-2X/6-311++G** calculations. T1 diagnostic calculations were performed to assess the multi-reference character of all stationary points. T1 diagnostic values for C_5H_6OH and C_5H_5OH are displayed in Table S1. Values are less than 0.02 for closed-shell species and less than 0.045 for open-shell species, indicating that multireference effects may be ignored for all electronic structures.[58,59] The atomic coordinates of the optimized structures, rotational constants, and vibrational frequencies for all stationary points are reported in Table S2.

3.2. Master Equation. Temporal profiles and branching fractions for the products of the OH + CPD reaction were calculated using the open-source Master Equation solver MESMER (Master Equation Solver for Multi Energy well Reactions).[60,61] MESMER solves coupled differential equations describing the reaction and energy transfer kinetics given stationary points of the PES. The methodology has been described in detail by Glowacki et al.[61] and has been employed to investigate OH radical reactions with unsaturated hydrocarbons[60] as well as CH radical reaction with ammonia[62] and cyclopentadiene.[47]

Isomerization and decomposition unimolecular rates of the reaction intermediates along the PES were calculated using Rice−Ramsperger−Kassel−Marcus (RRKM) theory. Energy transfer processes were modeled using a constant average energy transferred, ΔE_{down}. The classical rotor approximation

https://doi.org/10.1021/acs.jpca.2c06934
J. Phys. Chem. A 2022, 126, 9031−9041

was used for the reactants, whereas products were treated as quantum rotors using the 1D internal rotor potential from the M06-2X/6-311++G** scans. The energy grain size typically used for the modeling was 50 cm^{-1}, whereas a larger grain size of 100 cm^{-1} was used for the sensitivity analysis.[47] The energy grain was set to span a region possessing $20k_BT$ of energy in excess of the highest stationary point energy, where k_B is the Boltzmann constant and T is the temperature. The energy transfer and Lennard-Jones parameters (ε and σ) were taken from previous work on CH and OH reactions with unsaturated hydrocarbons. Values of σ = 4.3 Å and ε = 380 cm^{-1} were used for all the C_5H_6OH intermediates and σ = 2.55 Å and ε = 10.2 cm^{-1} for the He bath gas.[60,63,64] The collisional energy transfer parameter ΔE_{down} was kept independent of temperature at ΔE_{down} = 250 cm^{-1}. Calculations were also performed with ΔE_{down} = 300 cm^{-1} as suggested by Shannon et al.[60] in the reaction of OH with acetone and dimethyl ether. The final product branching fractions were found to be independent of the energy transfer parameters and grain size within the 300−1000 K and 4−1000 Torr temperature and pressure ranges. The initial cyclopentadiene number density was set to the experimental value.

4. EXPERIMENTAL RESULTS

Time- and energy-resolved mass spectra were recorded by averaging 300−800 laser shots at each VUV photon energy and scanned over the 7.3−9.0 eV energy range with 25 meV steps. The data were baseline subtracted for prephotolysis signals using the time range before each laser pulse and normalized for the VUV photon flux. Integrating the data over a given time range or energy range provides mass spectra that are either energy- or time-resolved. Positive ion signals in the mass spectra indicate species formed during and after the laser pulse. Photoion spectra were obtained by integrating the energy-resolved mass spectra over the mass species of interest. Isomeric species were identified based on their ionization energy (see Table 1) and through fitting the experimental photoion spectrum with simulated photoion spectra (integrated FCFs).

4.1. Vertical Ionization Energy. The reaction of OH with cyclopentadiene proceeds with a rate coefficient of 9.2 × 10^{-11} cm^{-3} s^{-1} at room temperature.[30,40] Assuming pseudo-first-order approximation and a cyclopentadiene number density of 5.7 × 10^{13} cm^{-3}, the characteristic time for the decay of the OH radical and rise of the primary products is of an order of 190 μs (rate of 5200 s^{-1}). Reactions of primary products with remaining radicals or other photoproducts in the flow may lead to the formation of secondary products over the experimental reaction time with a slower formation.[47,65] It is therefore possible to discriminate between primary and secondary reactions by integrating mass spectra and photoion spectra over the first few milliseconds of reaction time. Products showing a slow initial formation will have a smaller contribution to the spectra.

Data were recorded using both hydrogen peroxide and HONO as precursors at 248 and 351 nm photolysis, respectively. The absorption cross section of cyclopentadiene was previously reported as 4.5 × 10^{-18} cm^2 at 248 nm.[66] The energy- and time-resolved mass spectra of cyclopentadiene + 248 nm in He buffer gas have been previously recorded[47] at 373 K and 4 Torr and are used here to discriminate between OH + cyclopentadiene products and products resulting from cyclopentadiene photolysis. No cyclopentadiene absorption cross section values have been reported in the literature at 351 nm; however, at this wavelength, the molecule is not expected to photodissociate. In the following paragraphs, mass spectra, temporal traces, and photoion spectra from the 248 nm irradiation of a cyclopentadiene mixture with hydrogen peroxide are compared to those obtained from the 351 nm irradiation of a cyclopentadiene mixture with HONO to identify the primary product from the OH + cyclopentadiene reaction. Over the 4−8 Torr range, the pressure is found to have no observable effect on the time- and energy-resolved mass spectra. The data below are recorded at 4 or 8 Torr to present the most representative dataset.

Figure 1 displays the mass spectra obtained upon (a) 248 nm irradiation of a mixture containing H_2O_2 and cyclopentadiene at 4 Torr and 298 K and (b) 351 nm irradiation of a mixture containing HONO and cyclopentadiene at 8 Torr and 298 K. Signals at m/z 82, 83, and 84 are observed in both panels. Signals at m/z 80, 81, and 92 are detected only in the case of the 248 nm irradiation. The signals at m/z 80 and 92 were previously observed upon 248 nm irradiation of cyclopentadiene under similar conditions and were attributed to the reactant photodissociation and products from photoproduct reactions.[47] Below 9.0 eV, the signal at m/z 81 from CPD photodissociation is solely due to ^{13}C contribution from the m/z 80 signal. In Figure 1a, there is an additional contribution to the signal at m/z 81, likely from photolysis of an impurity, as indicated by its fast formation rate (see Table

Table 1. Structure, Name, Label, and CBS-QB3 Adiabatic Ionization Energies for C_5H_6OH (m/z 83) and C_5H_5OH (m/z 82) Isomers of Interest

structure/name	m/z	label	adiabatic ionization energy (eV)
 5-hydroxycyclopent-2-en-1-yl	83	INT1	7.31
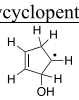 2-hydroxycyclopent-3-en-1-yl	83	INT2	8.22[(1)]
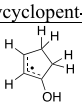 1-hydroxycyclopent-2-en-1-yl	83	INT5	6.17
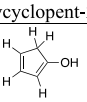 1,3-cyclopentadien-1-ol	82	P1	7.86
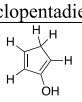 1,4-cyclopentadien-1-ol	82	P2	8.18
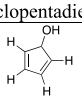 2,4-cyclopentadien-1-ol	82	P3	8.80

[a]Vertical ionization energy.

https://doi.org/10.1021/acs.jpca.2c06934
J. Phys. Chem. A 2022, 126, 9031−9041

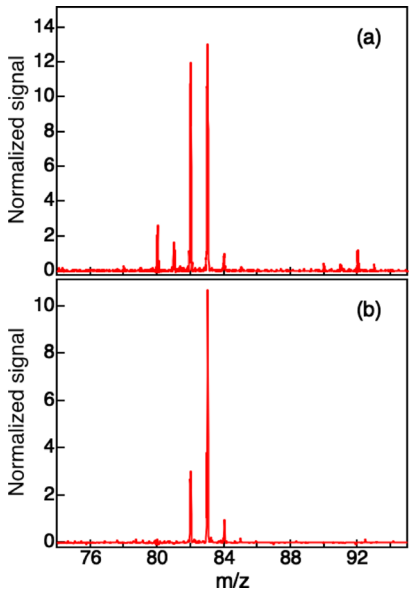

Figure 1. Mass spectra obtained upon (a) 248 nm irradiation of a mixture containing H_2O_2 and cyclopentadiene at 4 Torr and 298 K and (b) 351 nm irradiation of a mixture containing HONO and cyclopentadiene at 8 Torr and 298 K. In both panels, the ion signal is integrated over the 0−1 ms time range and 7.9−9.0 eV photon energy range.

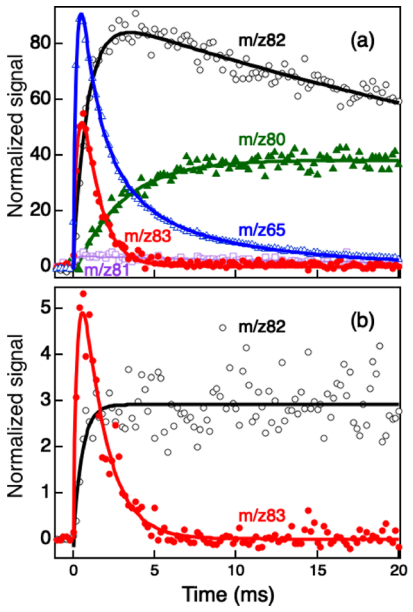

Figure 2. Temporal traces at m/z 65 (blue open triangles), 80 (green filled triangles), 81 (purple open squares), 82 (black open circles), and 83 (red filled circles) obtained upon (a) 248 nm irradiation of a mixture containing H_2O_2 and cyclopentadiene at 4 Torr and 298 K and (b) 351 nm irradiation of a mixture containing HONO and cyclopentadiene at 8 Torr and 298 K. The ion signal is integrated over the 7.9−9.0 eV photon energy range. The data are corrected for ^{13}C contribution. The solid lines are fit to the data using single or double exponential functions for product formation.

S3). Other detected signals outside of the m/z range of Figure 1a are consistent with 248 nm cyclopentadiene photoproducts (see Figure S2a,c).[47] Upon 351 nm irradiation, no significant laser-dependent signals are detected outside of the mass range displayed in Figure 1b (see Figure S2b). In particular, there is no evidence of cyclopentadienyl (C_5H_5, IE = 8.41 eV)[44] formation at m/z 65 (see Figure S3).

Figure 2 displays the temporal traces recorded at m/z 65, 80, 81, 82, and 83 obtained upon (a) 248 nm irradiation of a mixture containing H_2O_2 and cyclopentadiene at 4 Torr and 298 K and (b) 351 nm irradiation of a mixture containing HONO and cyclopentadiene at 8 Torr and 298 K. Temporal traces for signals observed upon irradiation of cyclopentadiene at 248 nm[47] are displayed in Figure S4. The ion signals are corrected for ^{13}C contribution. The solid lines are fit to the data using eq 1 corresponding to a pseudo-first order model of sequential reactions over the 0−20 ms time range,[67] where k_1 and k_2 are the rates for the rise and decay of the products, respectively, and S′ is the signal corresponding to the formation of the products.

$$S(t) = \left(\frac{S' \cdot k_1}{k_2 - k_1}\right) \cdot (e^{-k_1 \cdot t} - e^{-k_2 \cdot t}) \quad (1)$$

In the case of the m/z 65 signal, the fit includes a contribution from cyclopentadienyl self-reaction. This is achieved by fitting the signal to a system of two differential equations including a first-order formation (k_1) and decay (k_2) of cyclopentadienyl and a recombination contribution set to the experimental value.[68] The rate coefficients obtained from the fit are given in Table S3. Photolysis processes are found to be greater than the estimated instrument response function, 4000 s^{-1}.[69] The slower rise of the m/z 80 signal suggests that it results from secondary reactions of cyclopentadiene photoproducts. Signals at m/z 82 and 83 are found to have faster rises characteristic of a first-order radical reaction. Measuring the true formation rate would require deconvolving the signal rise with the instrument response function.[70] Nonetheless, the fast rise of the m/z 83 signal is consistent with its formation by reaction of OH with cyclopentadiene. The rise of m/z 82 signal is found to be very slow in the absence of OH precursors and remains consistently systematically slower than the expected instrument response function when OH precursors are added. This difference suggests that these two masses may be formed by different reactions. It is also unlikely that m/z 82 comes from decomposition of m/83 as the rise of the m/z 82 signal is consistently faster than the decay of m/z 83.

Figure 3 displays the photoion spectrum of m/z 83 (black markers) obtained upon 248 nm irradiation of a mixture

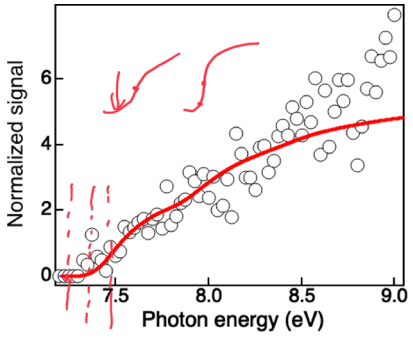

Figure 3. Photoion spectrum of m/z 83 (black markers) obtained upon 248 nm irradiation of a mixture containing H_2O_2 and cyclopentadiene at 4 Torr and 298 K over the 7.2−9.0 eV photon energy range. The ion signal is integrated over the 0−1 ms time range. The data are corrected for ^{13}C contribution. The red line is the integrated FCFs of 5-hydroxycyclopent-2-en-1-yl (INT1).

https://doi.org/10.1021/acs.jpca.2c06934
J. Phys. Chem. A 2022, 126, 9031−9041

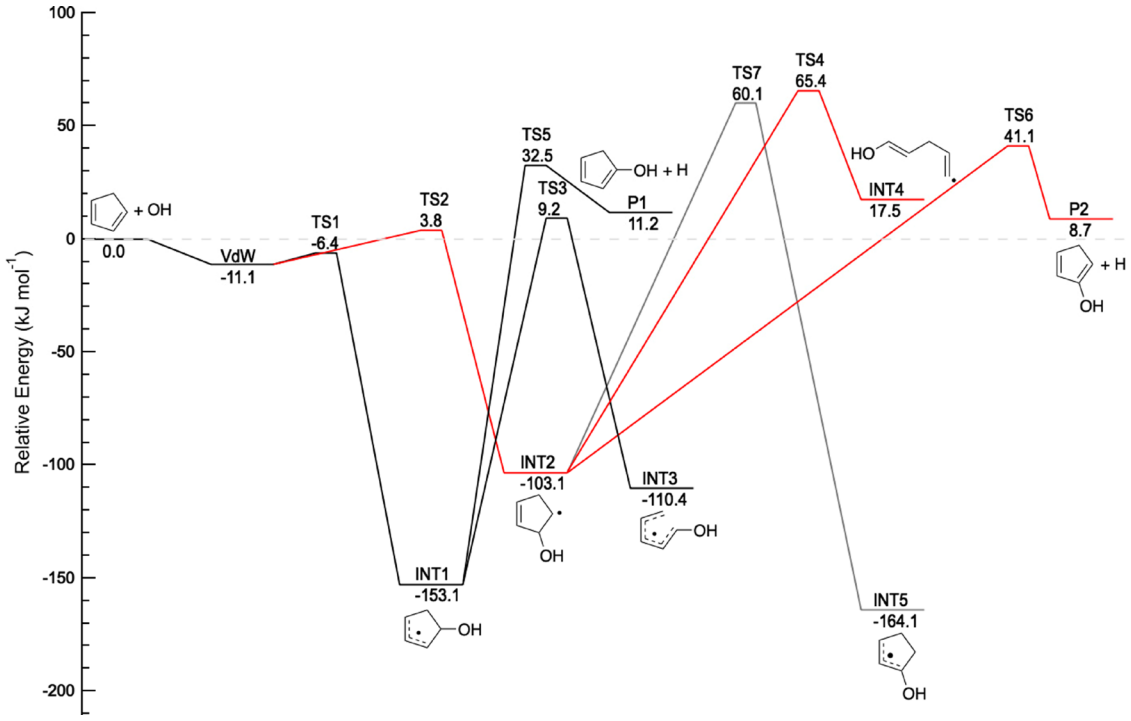

Figure 4. Part of the C_5H_6 + OH PES calculated using the CCSD(T)/cc-pVTZ//M06-2X/6-311++G** level of theory. The energies, corrected for zero-point energy (0 K), are given in kJ mol^{-1}.

containing H_2O_2 and cyclopentadiene at 4 Torr and 298 K. The data are corrected for ^{13}C contribution. Due to low overall photon flux below 8.0 eV combined with the low number density of the HONO precursor in the flow tube, the photoion spectra recorded upon 351 nm irradiation of a mixture containing HONO and cyclopentadiene show a very low signal (see Figure S5). Above 8.0 eV, the spectra recorded at 248 and 351 nm are similar. Given the similar rise and decay rates (see Table S3), it is assumed that the signals at *m/z* 83 are due to the same species in both 248 and 351 nm experiments. The ion onset in Figure 3 is 7.3 eV which matches the calculated adiabatic ionization energy of the 5-hydroxycyclopent-2-en-1-yl radical displayed in Table 1. The simulated photoion spectrum for INT1 is fitted to the experimental spectra from 7.3 to 7.8 eV to minimize the possible contribution from INT2. Because no *m/z* 83 ions are detected at 7.3 eV, the 1-hydroxycyclopent-2-en-1-yl isomer (INT5) with an adiabatic ionization energy of 6.17 eV is not detected. Deviation from the fit above 8.5 eV may be due to either the presence of INT2 or differences between the integrated FCF and the photoion spectrum of INT1. Such differences have been previously observed for unsaturated molecules.[71,72] The vertical ionization of 3-hydroxycyclopent-2-en-1-yl is calculated to be 8.22 eV which corresponds to the maximum of the photoelectron spectrum. Because the cation geometry cannot be optimized at the level of theory used in this study, FCFs for INT2 cannot be calculated. Nonetheless, the photoion spectrum can be approximated to that of INT1 with a shift in energy corresponding to the difference in vertical ionization between both isomers. Within this rough approximation, the *m/z* 83 spectra can be fit over the whole energy range. The fit is displayed in Figure S6 and results in a 3:2 branching ratio between INT1 and INT2. Although this method is likely to overestimate the fraction of INT2 formed, it suggests that INT2 may be a non-negligible reaction product.

Due to the slower *m/z* 82 signal rise, compared to that of *m/z* 83, C_5H_5OH isomers detected upon both 248 and 351 nm irradiation are unlikely to be formed by the OH + cyclopentadiene reaction. Signal at *m/z* 82 is also detected upon 248 nm irradiation of cyclopentadiene without OH precursors but with an ionization onset above 9.2 eV (see Figure S7), which is outside of the energy range used for the OH + cyclopentadiene study. Therefore, species at *m/z* 82 observed in Figure 1a,b must contain an oxygen atom from the OH radical. In addition, inspection of the high-resolution mass spectra for the present experiments reveals only one peak at *m/z* 82. The photoion spectrum integrated over the full time-range at *m/z* 82 (Figure S8) displays an ion onset at 7.8 eV for 248 nm irradiation and 8.1 eV for 351 nm irradiation. Although these values match the ionization onset of 1,3-cyclopentadien-1-ol (P1) and 1,4-cyclopentadien-1-ol (P2), the shape of the spectra does not match that of the integrated FCFs. Upon 248 nm irradiation, integrating the ion signal over the 0−2 ms time range leads to an ion onset at 7.8 eV, as reported above, while the ion onset shifts to ∼8.0 eV when integrating the signal over the 38−40 ms time range (see Figure S9). The *m/z* 82 photoion spectrum recorded with 351 nm irradiation is independent of integration time. The change of photoion spectra with reaction time observed upon 248 nm irradiation suggests that the *m/z* 82 signal is due to species formed by two different reactions. One of these reactions (also forming C_5H_5OH isomers at 351 nm) is not related to cyclopentadiene photodissociation. The second process, observed only upon 248 nm irradiation, is likely to be due to OH reaction with cyclopentadiene photoproducts.

5. DISCUSSION

The detection of *m/z* 83 with a fast rise time upon irradiation of a cyclopentadiene mixture with both H_2O_2 at 248 nm and HONO at 351 nm suggests that C_5H_6OH isomers are formed

https://doi.org/10.1021/acs.jpca.2c06934
J. Phys. Chem. A 2022, 126, 9031−9041

by reaction of the OH radical with cyclopentadiene. Isomers of C_5H_5OH at m/z 82 seem to be formed in the reaction flow by slower side reactions rather than by H-atom loss from the m/z 83 C_5H_6OH radical. Analysis of the C_5H_6OH photoion spectra suggests that 5-hydroxycyclopent-2-en-1-yl (INT1) is the only isomer contributing to the ion signal. Upon irradiation at 351 nm, no signal is observed at m/z 65, indicating that cyclopentadienyl is not formed in the reaction flow. These results strongly suggest that at room temperature and over the 4−8 Torr pressure range, formation of INT1 by OH addition to cyclopentadiene is the sole reaction pathway.

Figure 4 displays part of the C_5H_6OH PES calculated using the CCSD(T)/cc-pVTZ//M06-2X/6-311++G** level of theory. The energies are similar to those recently calculated by Mai et al.[42] at the M06-2X/aug-cc-pVTZ level of theory. The reaction is found to proceed through the initial barrierless formation of a VdW complex. The VdW complex isomerizes to the resonance stabilized INT1 and to INT2 through TS1 and TS2, respectively. At this level of theory, the energy of TS2 is found to be slightly higher than the reactant energies, while that of TS1 is found to be lower. This difference in energy is likely due to the development of resonance stabilization at the geometry of TS1. Both INT1 and INT2 energies are well below those of the reactants, with INT1 being more stable by 50 kJ mol^{-1} due to resonance stabilization. H-loss from INT1 and INT2 forms OH substitution products P1 and P2 through TS5 and TS6, respectively. The energies of the products and of the transition states are all significantly above those of the reactants. Product P3 (see Table 1) is found to have an energy 42.4 kJ mol^{-1} above those of the reactants (not displayed in Figure 4) and is not considered a competitive channel compared to the other bimolecular product channels. Alternatively, INT1 can ring open to form the resonance-stabilized INT3 through TS3, 9.2 kJ mol^{-1} above the energy of the reactants. Ring opening from INT2 forms a non-resonance-stabilized radical through TS4, 65.4 kJ mol^{-1} above the energy of the reactants. H-losses from the noncyclic INT3 and INT4 were not investigated as they are unlikely to be significant under the pressure and temperature conditions investigated here. INT2 can isomerize to the resonance-stabilized INT5 by H-atom transfer. Although this radical is the most stable intermediate on the calculated PES, its formation involves an energy barrier 60.1 kJ mol^{-1} above the energy of the reactants.

The PES displayed in Figure 4 suggests that the resonance-stabilized INT1 may be formed by addition of the OH radical to either carbon 2 or 5 of the cyclopentadiene reactant (Scheme 1) through a submerged energy barrier. All other pathways have saddle points with energy above those of the reactants and are unlikely to dominate at room temperature. To further investigate the formation of the C_5H_6OH and C_5H_5OH isomers in the reaction flow, RRKM-based ME calculations were run using the open-source software MESMER.[61] All the addition channels displayed in Figure 4 were included in the calculations. Figure 5 displays the calculated temporal profiles at (a) 298 K and (b) 1000 K for INT1 (red line), INT2 (green line), P1 (black line), and P2 (blue line) at 4 Torr. The other isomer intermediates are formed with negligible fractions. At room temperature and 4 Torr, the Master Equation finds that stabilization of the resonance-stabilized INT1 is the sole reaction product, in agreement with a recent computational study.[42] The probable detection of INT2 in our experiment may suggest uncertainties

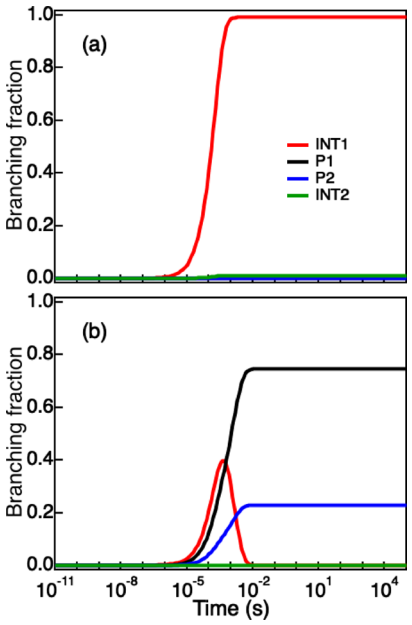

Figure 5. MESMER-calculated temporal profiles of INT1 (red line), INT2 (green line), P1 (black line), and P2 (blue line) from reaction of the OH radical with cyclopentadiene at (a) 298 K and (b) 1000 K at 4 Torr.

about the energy barrier height for isomerization of the VdW complex to INT2. Calculations at a higher level of theory are required to resolve this discrepancy. Nonetheless, the ME calculations qualitatively agree with the experimental findings. At higher temperatures, cyclopentadien-2-ol + H (P1) and cyclopentadien-3-ol + H (P2) become the dominant reaction products with branching fractions of 0.76 and 0.24, respectively, at 1000 K. At such high temperatures, however, H-abstraction to form cyclopentadienyl (C_5H_5) + H_2O is likely to become the dominant reaction pathway as suggested by the recent kinetic[30] and ME studies.[42] The temperature and pressure dependences of the addition and abstraction branching ratios have been calculated by Mai et al.[42]

The detection of the stabilized adduct for the OH + cyclopentadiene reaction validates the previously proposed mechanism for addition of the OH onto conjugated hydrocarbons[24,32,42] as displayed in Scheme 2. The addition of the OH radical onto one of the terminal vinylic carbons (labeled 1 and 4) forms an RSR. This radical is likely to accumulate in gas-phase environments due to its resistance to reaction with

Scheme 2. General Reaction Mechanism for OH Addition to Conjugated Hydrocarbons

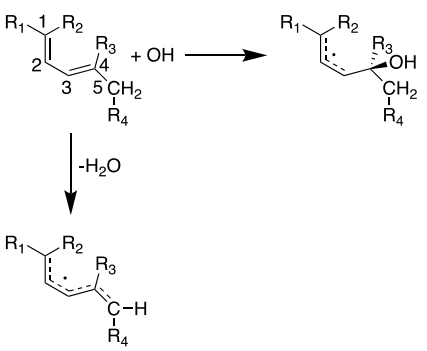

https://doi.org/10.1021/acs.jpca.2c06934
J. Phys. Chem. A 2022, 126, 9031−9041

molecular oxygen, as mentioned in the Introduction. The OH addition onto the carbons labeled 2 and 3 is expected to be less favorable than onto the terminal vinylic carbons because the resulting intermediates are not stabilized by resonance. Abstraction of a hydrogen atom will compete with the formation of the addition adduct, although the temperature at which this channel becomes dominant depends on the overall structure of the molecule. The hydrogen atoms on the carbon labeled 5 are doubly allylic, and their abstraction will lead to an RSR. The substituent groups R1 and R2 may also participate in the conjugation, making the formed radical very stable. The increased resonance stabilization could lower the energy of the transition state, making abstraction a competitive channel at lower temperatures. In the case of cyclopentadiene, the sp^3 hybridized carbon (carbon 1 in Scheme 1) has two doubly allylic C−H bonds that will lead to the RSR cyclopentadienyl upon H-atom abstraction.

6. CONCLUSIONS

The present study provides the first experimental evidence for formation of the resonance-stabilized 5-hydroxycyclopent-2-en-1-yl (C_5H_6OH) by reaction of the OH radical with cyclopentadiene. Its direct detection validates recent computational studies on the OH + cyclopentadiene reaction.[42] The detection of such elusive species under multiple collision conditions is facilitated by its long reaction lifetime, the use of a soft ionization technique, and its deep energetic well on the PES from resonance stabilization. The calculated PES shows that OH addition to form the RSR proceeds through a submerged energy barrier, making this mechanism favorable at low temperatures. All other addition pathways are found to have energy barriers above the energy of the reactants and may open at temperatures higher than 500 K.[42]

In combustion environments, abstraction is likely to be the dominant reaction mechanism.[30,42] In addition, at high temperatures, the addition pathway primarily leads to the formation of the H-substitution products, 1,3-cyclopentadien-1-ol and 1,4-cyclopentadien-1-ol, through subsequent H-loss. The OH + cyclopentadiene reaction is therefore unlikely to be a significant source of the RSR 5-hydroxycyclopent-2-en-1-yl in combustion flames. Nonetheless, OH-containing RSRs are likely to be formed by other pathways[1,5] and the present study highlights the stability of such species. At and below room temperature, the abstraction mechanism is slow and addition products dominate. With the recent detection of cyclopentadiene and cyano-cyclopentadiene in the ISM,[38,39] cyclopentadiene chemistry is likely to contribute to the low-temperature chemical scheme in ISM environments. The OH + cyclopentadiene reaction at low temperatures will lead to the formation of the resonance-stabilized 5-hydroxycyclopent-2-en-1-yl. Under the experimental conditions, collisional quenching is very efficient, and the detected molecules are all fully thermalized to the flow conditions. In the ISM, once formed under low-pressure conditions, the 5-hydroxycyclopent-2-en-1-yl radical is unlikely to undergo any further unimolecular isomerization or dissociation. Depending on the lifetime of the RSR, it could either decompose back to the reactants or be stabilized by vibrational relaxation. The radical could then further react by reaction with other abundant species in the gas phase or on surfaces. Such OH-containing RSRs will contribute to molecular weight growth as well as to the incorporation of oxygen into large hydrocarbon species and particles.

The proposed mechanism for addition of the OH radical to cyclopentadiene may be extended to other unsaturated conjugated hydrocarbons to form RSRs. This mechanism is likely to be a significant source of RSRs in the atmosphere by reaction of the OH radical with molecules such as isoprene, acrolein, and conjugated cyclic ketones. Further experimental and theoretical investigations are therefore necessary to fully understand the role of OH-containing RSRs in gas-phase chemistry.

■ ASSOCIATED CONTENT

Supporting Information

The Supporting Information is available free of charge at https://pubs.acs.org/doi/10.1021/acs.jpca.2c06934.

Hindered-rotor potentials of the 5-hydroxycyclopent-2-en-1-yl neutral and cationic species, T1 diagnostic values, vibrational frequencies, rotational constants, and atomic coordinates of the reactants and intermediates, mass spectra over a wider mass range, fitted first-order rate coefficients, product kinetic traces without OH precursors, and photoion spectra of photoproducts and reaction products under different integration conditions (PDF)

■ AUTHOR INFORMATION

Corresponding Author

Fabien Goulay − *C. Eugene Bennett Department of Chemistry, West Virginia University, Morgantown, West Virginia 26506, United States;* orcid.org/0000-0002-7807-1023; Email: Fabien.Goulay@mail.wvu.edu

Authors

Kacee L. Caster − *C. Eugene Bennett Department of Chemistry, West Virginia University, Morgantown, West Virginia 26506, United States;* orcid.org/0000-0001-6926-9209

James Lee − *C. Eugene Bennett Department of Chemistry, West Virginia University, Morgantown, West Virginia 26506, United States*

Zachery Donnellan − *C. Eugene Bennett Department of Chemistry, West Virginia University, Morgantown, West Virginia 26506, United States*

Talitha M. Selby − *Department of Mathematics and Natural Sciences, University of Wisconsin-Milwaukee, West Bend, Wisconsin 53095, United States*

David L. Osborn − *Combustion Research Facility, Sandia National Laboratories, Livermore, California 94551, United States; Department of Chemical Engineering, University of California, Davis, Davis, California 95616, United States;* orcid.org/0000-0003-4304-8218

Complete contact information is available at: https://pubs.acs.org/10.1021/acs.jpca.2c06934

Notes

The authors declare no competing financial interest.

■ ACKNOWLEDGMENTS

F.G., K.L.C., J.L., and Z.D. are grateful to the National Science Foundation for its support of this work through Grant CHE-1764178. They also acknowledge travel support from the Eberly College of Art and Sciences and the C. Eugene Bennett Department of Chemistry at West Virginia University. The

authors also thank the West Virginia University High Performance Computing shared facility for providing computing resources. T.M.S. thanks the Washington County Campus Foundation and the College of General Studies for financial support for this research. The authors thank Raybel Almeida for technical support of this experiment and Dr. Adam Trevitt for his help with setting up of the HONO generator. D.L.O. and the instrumentation for this work are supported by the Division of Chemical Sciences, Geosciences, and Biosciences, the Office of Basic Energy Sciences, the U.S. Department of Energy. Sandia National Laboratories is a multi-mission laboratory managed and operated by National Technology and Engineering Solutions of Sandia, LLC, a wholly owned subsidiary of Honeywell International, Inc. for the U.S. DOE's National Nuclear Security Administration under contract DE-NA0003525. This paper describes objective technical results and analysis. Any subjective views or opinions that might be expressed in the paper do not necessarily represent the views of the USDOE or the United States Government. This research used resources of the Advanced Light Source, a DOE Office of Science User Facility, which is supported by the Direct, Office of Science, Office of Basic Energy Sciences, the U.S. Department of Energy under contract DE-AC02-05CH11231 at Lawrence Berkeley National Laboratory.

REFERENCES

(1) Troy, T. P.; Nakajima, M.; Chalyavi, N.; Nauta, K.; Kable, S. H.; Schmidt, T. W. Hydroxyl Addition to Aromatic Alkenes: Resonance-Stabilized Radical Intermediates. *J. Phys. Chem. A* **2012**, *116*, 7906−7915.

(2) Abhinavam Kailasanathan, R. K.; Thapa, J.; Goulay, F. Kinetic study of the OH radical reaction with Phenylacetylene. *J. Phys. Chem. A* **2014**, *118*, 7732−7741.

(3) Allodi, M. A.; Kirschner, K. N.; Shields, G. C. Thermodynamics of the hydroxyl radical addition to isoprene. *J. Phys. Chem. A* **2008**, *112*, 7064−7071.

(4) Daranlot, J.; Hickson, K. M.; Loison, J.-C.; Mereau, R.; Caralp, F.; Forst, W.; Bergeat, A. Gas-Phase Kinetics of the Hydroxyl Radical Reaction with Allene: Absolute Rate Measurements at Low Temperature, Product Determinations, and Calculations. *J. Phys. Chem. A* **2012**, *116*, 10871−10881.

(5) Wilcox, C. M.; Krechkivska, O.; Nauta, K.; Schmidt, T. W.; Kahle, S. H. Jet-Cooled Spectroscopy of ortho-Hydroxycyclohexadienyl Radicals. *J. Phys. Chem. A* **2018**, *122*, 8886−8897.

(6) Johansson, K. O.; Head-Gordon, M. P.; Schrader, P. E.; Wilson, K. R.; Michelsen, H. A. Resonance-stabilized hydrocarbon-radical chain reactions may explain soot inception and growth. *Science* **2018**, *361*, 997−1000.

(7) Wang, K.; Villano, S. M.; Dean, A. M. Ab initio study of the influence of resonance stabilization on intramolecular ring closure reactions of hydrocarbon radicals. *Phys. Chem. Chem. Phys.* **2016**, *18*, 8437−8452.

(8) Schmidt, T. W. The electronic spectroscopy of resonance-stabilised hydrocarbon radicals. *Int. Rev. Phys. Chem.* **2016**, *35*, 209−242.

(9) Scheer, A. M.; Eskola, A. J.; Osborn, D. L.; Sheps, L.; Taatjes, C. A. Resonance Stabilization Effects on Ketone Autoxidation: Isomer-Specific Cyclic Ether and Ketohydroperoxide Formation in the Low-Temperature (400-625 K) Oxidation of Diethyl Ketone. *J. Phys. Chem. A* **2016**, *120*, 8625−8636.

(10) Scheer, A. M.; Welz, O.; Zador, J.; Osborn, D. L.; Taatjes, C. A. Low-temperature combustion chemistry of novel biofuels: resonance-stabilized QOOH in the oxidation of diethyl ketone. *Phys. Chem. Chem. Phys.* **2014**, *16*, 13027−13040.

(11) Reilly, N. J.; Kokkin, D. L.; Nakajima, M.; Nauta, K.; Kable, S. H.; Schmidt, T. W. Spectroscopic observation of the resonance-stabilized 1-phenylpropargyl radical. *J. Am. Chem. Soc.* **2008**, *130*, 3137−3142.

(12) Zador, J.; Taatjes, C. A.; Fernandes, R. X. Kinetics of elementary reactions in low-temperature autoignition chemistry. *Prog. Energy Combust. Sci.* **2011**, *37*, 371−421.

(13) Hippler, H.; Reihs, C.; Troe, J. Shock tube UV absorption study of the oxidation of benzyl radicals. *Proc. Combust. Inst.* **1991**, *23*, 37−43.

(14) Hahn, D. K.; Klippenstein, S. J.; Miller, J. A. A theoretical analysis of the reaction between propargyl and molecular oxygen. *Faraday Discuss.* **2001**, *119*, 79−100.

(15) da Silva, G.; Bozzelli, J. W. The C7H5 Fulvenallenyl Radical as a Combustion Intermediate: Potential New Pathways to Two- and Three-Ring PAHS. *J. Phys. Chem. A* **2009**, *113*, 12045−12048.

(16) Mebel, A. M.; Kislov, V. V. Can the $C_5H_5 + C_5H_5 \rightarrow C_{10}H_{10} \rightarrow C_{10}H_9 + H/C_{10}H_8 + H_2$ Reaction Produce Naphthalene? An Ab Initio/RRKM Study. *J. Phys. Chem. A* **2009**, *113*, 9825−9833.

(17) Cavallotti, C.; Polino, D. On the kinetics of the $C_5H_5 + C_5H_5$ reaction. *Proc. Combust. Inst.* **2013**, *34*, 557−564.

(18) Matsugi, A.; Miyoshi, A. Modeling of two- and three-ring aromatics formation in the pyrolysis of toluene. *Proc. Combust. Inst.* **2013**, *34*, 269−277.

(19) Sinha, S.; Raj, A. Polycyclic aromatic hydrocarbon (PAH) formation from benzyl radicals: a reaction kinetics study. *Phys. Chem. Chem. Phys.* **2016**, *18*, 8120−8131.

(20) Hansen, N.; Cool, T. A.; Westmoreland, P. R.; Kohse-Hoinghaus, K. Recent contributions of flame-sampling molecular-beam mass spectrometry to a fundamental understanding of combustion chemistry. *Prog. Energy Combust Sci.* **2009**, *35*, 168−191.

(21) Hansen, N.; Miller, J. A.; Klippenstein, S. J.; Westmoreland, P. R.; Kohse-Hoinghaus, K. Exploring formation pathways of aromatic compounds in laboratory-based model flames of aliphatic fuels. *Combust. Explos. Shock Waves* **2012**, *48*, 508−515.

(22) Martin, J. W.; Salamanca, M.; Kraft, M. Soot inception: Carbonaceous nanoparticle formation in flames. *Prog. Energy Combust. Sci.* **2022**, *88*, No. 100956.

(23) Ghosh, B.; Bugarin, A.; Connell, B. T.; North, S. W. Isomer-Selective Study of the OH-Initiated Oxidation of Isoprene in the Presence of O-2 and NO: 2. The Major OH Addition Channel. *J. Phys. Chem. A* **2010**, *114*, 2553−2560.

(24) Greenwald, E. E.; North, S. W.; Georgievskii, Y.; Klippenstein, S. J. A two transition state model for radical-molecule reactions: Applications to isomeric branching in the OH-Isoprene reaction. *J. Phys. Chem. A* **2007**, *111*, 5582−5592.

(25) Loison, J.-C.; Daranlot, J.; Bergeat, A.; Caralp, F.; Mereau, R.; Hickson, K. M. Gas-Phase Kinetics of Hydroxyl Radical Reactions with C_3H_6 and C_4H_8: Product Branching Ratios and OH Addition Site-Specificity. *J. Phys. Chem. A* **2010**, *114*, 13326−13336.

(26) Magneron, I.; Thevenet, R.; Mellouki, A.; Le Bras, G.; Moortgat, G. K.; Wirtz, K. A study of the photolysis and OH-initiated oxidation of acrolein and trans-crotonaldehyde. *J. Phys. Chem. A* **2002**, *106*, 2526−2537.

(27) Senosiain, J. P.; Klippenstein, S. J.; Miller, J. A. Oxidation pathways in the reaction of diacetylene with OH radicals. *Proc. Combust. Inst.* **2007**, *31*, 185−192.

(28) Peeters, J.; Boullart, W.; Pultau, V.; Vandenberk, S.; Vereecken, L. Structure-activity relationship for the addition of OH to (poly)alkenes: Site-specific and total rate constants. *J. Phys. Chem. A* **2007**, *111*, 1618−1631.

(29) Zador, J.; Miller, J. A. Adventures on the C_3H_5O potential energy surface: OH plus propyne, OH plus allene and related reactions. *Proc. Combust. Inst.* **2015**, *35*, 181−188.

(30) Jin, H. F.; Liu, D. P.; Zou, J. B.; Hao, J. Y.; Shao, C.; Sarathy, S. M.; Farooq, A. Chemical kinetics of hydroxyl reactions with cyclopentadiene and indene. *Combust. Flame* **2020**, *217*, 48−56.

(31) Greenwald, E.; North, S.; Georgievskii, Y.; Klippenstein, S. A two transition state model for radical−molecule reactions: A case study of the addition of OH to C_2H_4. *J. Phys. Chem. A* **2005**, *109*, 6031−6044.

https://doi.org/10.1021/acs.jpca.2c06934
J. Phys. Chem. A 2022, 126, 9031−9041

(32) Greenwald, E. E.; Ghosh, B.; Anderson, K. C.; Dooley, K. S.; Zou, P.; Selby, T.; Osborn, D. L.; Meloni, G.; Taatjes, C. A.; Goulay, F.; North, S. W. Isomer-Selective Study of the OH Initiated Oxidation of Isoprene in the Presence of O_2 and NO. I. The Minor Inner OH-Addition Channel. *J. Phys. Chem. A* **2010**, *114*, 904−912.
(33) Illmann, N.; Gibilisco, R. G.; Bejan, I. G.; Patroescu-Klotz, I.; Wiesen, P. Atmospheric oxidation of alpha,beta-unsaturated ketones: kinetics and mechanism of the OH radical reaction. *Atmos. Chem. Phys.* **2021**, *21*, 13667−13686.
(34) Orlando, J. J.; Tyndall, G. S. Mechanisms for the reactions of OH with two unsaturated aldehydes: Crotonaldehyde and acrolein. *J. Phys. Chem. A* **2002**, *106*, 12252−12259.
(35) Brezinsky, K. The high-temperature oxidation of aromatic hydrocarbons. *Prog. Energy Combust. Sci.* **1986**, *12*, 1−24.
(36) Vandewiele, N. M.; Magoon, G. R.; Van Geem, K. M.; Reyniers, M. F.; Green, W. H.; Marin, G. B. Experimental and Modeling Study on the Thermal Decomposition of Jet Propellant-10. *Energy Fuels* **2014**, *28*, 4976−4985.
(37) Cernicharo, J.; Agundez, M.; Cabezas, C.; Tercero, B.; Marcelino, N.; Pardo, J. R.; de Vicente, P. Pure hydrocarbon cycles in TMC-1: Discovery of ethynyl cyclopropenylidene, cyclopentadiene, and indene. *Astron. Astrophys* **2021**, *649*, L15.
(38) McCarthy, M. C.; Lee, K. L. K.; Loomis, R. A.; Burkhardt, A. M.; Shingledecker, C. N.; Charnley, S. B.; Cordiner, M. A.; Herbst, E.; Kalenskii, S.; Willis, E. R.; et al. Interstellar detection of the highly polar five-membered ring cyanocyclopentadiene. *Nat. Astron.* **2021**, *5*, 176−180.
(39) Lee, K. L. K.; Changala, P. B.; Loomis, R. A.; Burkhardt, A. M.; Xue, C.; Cordiner, M. A.; Charnley, S. B.; McCarthy, M. C.; McGuire, B. A. Interstellar Detection of 2-cyanocyclopentadiene, C_5H_5CN, a Second Five-membered Ring toward TMC-1. *Astrophys. J. Lett* **2021**, *910*, L2.
(40) Grosjean, D.; Williams, E. L. Environmental persistence of organic-compounds estimated from structure reactivity and linear free-energy relationship unsaturated aliphatics. *Atmos. Environ. A Gen. Topics* **1992**, *26*, 1395−1405.
(41) Wang, H. Y.; Liu, Z. Q.; Gong, S. Y.; Liu, Y. J.; Wang, L.; Zhang, X. W.; Liu, G. Z. Experimental and kinetic modeling study on 1,3-cyclopentadiene oxidation and pyrolysis. *Combust. Flame* **2020**, *212*, 189−204.
(42) Mai, T. V.-T.; Nguyen, H. D.; Nguyen, P.-D.; Nguyen, H. T.; Na, O. M.; Le, T. H.-M.; Huynh, L. K. Ab initio kinetics of OH-initiated oxidation of cyclopentadiene. *Fuel* **2022**, *317*, No. 123305.
(43) Brynteson, M. D.; Womack, C. C.; Booth, R. S.; Lee, S. H.; Lin, J. J.; Butler, L. J. Radical Intermediates in the Addition of OH to Propene: Photolytic Precursors and Angular Momentum Effects. *J. Phys. Chem. A* **2014**, *118*, 3211−3229.
(44) Manion, J. A.; Huie, R. E.; Levin, R. D.; Burgess, Jr., D. R.; Orkin, V. L.; Tsang, W.; McGivern, W. S.; Hudgens, J. W.; Knyazev, V. D.; Atkinson, D. B.; et al.*NIST Standard Reference Database 17*; National Institute of Standards and Technology, 2008. http://kinetics.nist.gov/ (accessed 2022).
(45) Osborn, D. L.; Zou, P.; Johnsen, H.; Hayden, C. C.; Taatjes, C. A.; Knyazev, V. D.; North, S. W.; Peterka, D. S.; Ahmed, M.; Leone, S. R. The multiplexed chemical kinetic photoionization mass spectrometer: A new approach to isomer-resolved chemical kinetics. *Rev. Sci. Instrum* **2008**, *79*, 104103.
(46) Taatjes, C. A.; Hansen, N.; Osborn, D. L.; Kohse-Hoeinghaus, K.; Cool, T. A.; Westmoreland, P. R. "Imaging" combustion chemistry via multiplexed synchrotron-photoionization mass spectrometry. *Phys. Chem. Chem. Phys.* **2008**, *10*, 20−34.
(47) Caster, K. L.; Selby, T. M.; Osborn, D. L.; Le Picard, S. D.; Goulay, F. Product Detection of the $CH(X^2\Pi)$ Radical Reaction with Cyclopentadiene: A Novel Route to Benzene. *J. Phys. Chem. A* **2021**, *125*, 6927−6939.
(48) Egerton, A. C.; Emte, W.; Minkoff, G. J. SOME PROPERTIES OF ORGANIC PEROXIDES. *Disc. Faraday Soc.* **1951**, *10*, 278−282.
(49) Molina, L. T.; Molina, M. J. UV absorption cross-section of $H_2O_2NO_2$ vapor. *J. Photochem.* **1981**, *15*, 97−108.
(50) Ray, A. W.; Taatjes, C. A.; Welz, O.; Osborn, D. L.; Meloni, G. Synchrotron Photoionization Measurements of OH-Initiated Cyclohexene Oxidation: Ring-Preserving Products in OH plus Cyclohexene and Hydroxycyclohexyl plus O-2 Reactions. *J. Phys. Chem. A* **2012**, *116*, 6720−6730.
(51) Frisch, M. J.; Trucks, G. W.; Schlegel, H. B.; Scuseria, G. E.; Robb, M. A.; Cheeseman, J. R.; Scalmani, G.; Barone, V.; Petersson, G. A.; Nakatsuji, H.; et al.*Gaussian 16 Rev. C.01*; Gaussian, Inc.: Wallingford, CT, 2016.
(52) Zhao, Y.; Truhlar, D. G. The M06 suite of density functionals for main group thermochemistry, thermochemical kinetics, noncovalent interactions, excited states, and transition elements: two new functionals and systematic testing of four M06-class functionals and 12 other functionals. *Theor. Chem. Acc.* **2008**, *120*, 215−241.
(53) Sheps, L.; Dewyer, A. L.; Demireva, M.; Zador, J. Quantitative Detection of Products and Radical Intermediates in Low-Temperature Oxidation of Cyclopentane. *J. Phys. Chem. A* **2021**, *125*, 4467−4479.
(54) Becke, A. D. A new mixing of Hartree-Fock and local density-functional theories. *J. Chem. Phys.* **1993**, *98*, 1372−1377.
(55) Montgomery, J.; Frisch, M.; Ochterski, J.; Peterson, G. A complete basis set model chemistry VII. Use of the minimum population localization method. *J. Chem. Phys.* **2000**, *112*, 6532−6542.
(56) Barone, V.; Bloino, J.; Biczysko, M.; Santoro, F. Fully Integrated Approach to Compute Vibrationally Resolved Optical Spectra: From Small Molecules to Macrosystems. *J. Chem. Theo. Comp.* **2009**, *5*, 540−554.
(57) Voronova, K.; Ervin, K. M.; Torma, K. G.; Hemberger, P.; Bodi, A.; Gerber, T.; Osborn, D. L.; Sztaray, B. Radical Thermometers, Thermochemistry, and Photoelectron Spectra: A Photoelectron Photoion Coincidence Spectroscopy Study of the Methyl Peroxy Radical. *J. Phys. Chem. Lett.* **2018**, *9*, 534−539.
(58) Alecu, I. M.; Truhlar, D. G. Computational Study of the Reactions of Methanol with the Hydroperoxyl and Methyl Radicals. 1. Accurate Thermochemistry and Barrier Heights. *J. Phys. Chem. A* **2011**, *115*, 2811−2829.
(59) Yao, X. X.; Pang, W. Q.; Li, T.; Shentu, J. T.; Li, Z. R.; Zhu, Q.; Li, X. Y. High-Pressure-Limit and Pressure-Dependent Rate Rules for Unimolecular Reactions Related to Hydroperoxy Alkyl Radicals in Normal-Alkyl Cyclohexane Combustion. 2. Cyclization Reaction Class. *J. Phys. Chem. A* **2021**, *125*, 8959−8977.
(60) Shannon, R. J.; Caravan, R. L.; Blitz, M. A.; Heard, D. E. A combined experimental and theoretical study of reactions between the hydroxyl radical and oxygenated hydrocarbons relevant to astrochemical environments. *Phys. Chem. Chem. Phys.* **2014**, *16*, 3466−3478.
(61) Glowacki, D. R.; Liang, C.-H.; Morley, C.; Pilling, M. J.; Robertson, S. H. MESMER: An Open-Source Master Equation Solver for Multi-Energy Well Reactions. *J. Phys. Chem. A* **2012**, *116*, 9545−9560.
(62) Blitz, M. A.; Talbi, D.; Seakins, P. W.; Smith, I. W. M. Rate Constants and Branching Ratios for the Reaction of CH Radicals with NH_3: A Combined Experimental and Theoretical Study. *J. Phys. Chem. A* **2012**, *116*, 5877−5885.
(63) Pakhira, S.; Singh, R. I.; Olatunji-Ojo, O.; Frenklach, M.; Lester, W. A. Quantum Monte Carlo Study of the Reactions of CH with Acrolein: Major and Minor Channels. *J. Phys. Chem. A* **2016**, *120*, 3602−3612.
(64) Pakhira, S.; Lengeling, B. S.; Olatunji-Ojo, O.; Caffarel, M.; Frenklach, M.; Lester, W. A. A Quantum Monte Carlo Study of the Reactions of CH with Acrolein. *J. Phys. Chem. A* **2015**, *119*, 4214−4223.
(65) Bourgalais, J.; Caster, K.; Durif, O.; Osborn, D. L.; Le Picard, S. D.; Goulay, F. Product Detection of the CH Radical Reactions with Ammonia and Methyl-Substituted Amines. *J. Phys. Chem. A* **2019**, *123*, 2178−2193.
(66) Cai, W.; Powell, C. F.; Yue, Y.; Narayanan, S.; Tate, M. W.; Renzi, M. J.; Ercan, A.; Fontes, E.; Gruner, S. M. Quantitative analysis of highly transient fuel sprays by time-resolved x-radiography. *Appl. Phys. Lett.* **2003**, *83*, 1671−1673.

https://doi.org/10.1021/acs.jpca.2c06934
J. Phys. Chem. A 2022, 126, 9031−9041

(67) Bourgalais, J.; Spencer, M.; Osborn, D. L.; Goulay, F.; Le Picard, S. D. Reactions of Atomic Carbon with Butene Isomers: Implications for Molecular Growth in Carbon-Rich Environments. *J. Phys. Chem. A* **2016**, *120*, 9138−9150.
(68) Knyazev, V. A.; Popov, K. Kinetics of the Self Reaction of Cyclopentadienyl Radicals. *J. Phys. Chem. A* **2015**, *119*, 7418−7429.
(69) Welz, O.; Savee, J. D.; Osborn, D. L.; Vasu, S. S.; Percival, C. J.; Shallcross, D. E.; Taatjes, C. A. Direct Kinetic Measurements of Criegee Intermediate (CH_2OO) Formed by Reaction of CH_2I with O_2. *Science* **2012**, *335*, 204−207.
(70) Eskola, A. J.; Dontgen, M.; Rotavera, B.; Caravan, R. L.; Welz, O.; Savee, J. D.; Osborn, D. L.; Shallcross, D. E.; Percival, C. J.; Taatjes, C. A. Direct kinetics study of CH_2OO + methyl vinyl ketone and CH_2OO + methacrolein reactions and an upper limit determination for CH_2OO + CO reaction. *Phys. Chem. Chem. Phys.* **2018**, *20*, 19373−19381.
(71) Goulay, F.; Derakhshan, A.; Maher, E.; Trevitt, A. J.; Savee, J. D.; Scheer, A. M.; Osborn, D. L.; Taatjes, C. A. Formation of dimethylketene and methacrolein by reaction of the CH radical with acetone. *Phys. Chem. Chem. Phys.* **2013**, *15*, 4049−4058.
(72) Xu, H.; Jacovella, U.; Ruscic, B.; Pratt, S. T.; Lucchese, R. R. Near-threshold shape resonance in the photoionization of 2-butyne. *J. Chem. Phys* **2012**, *136*, 154303.

https://doi.org/10.1021/acs.jpca.2c06934
J. Phys. Chem. A 2022, 126, 9031−9041